AGU ADVANCING EARTH AND SPACE SCIENCES

Water Resources Research

RESEARCH ARTICLE
10.1029/2025WR040153

Effective Thermal Retardation in Aquifers of Heterogeneous Hydraulic Conductivity

Hannah Gebhardt[1], **Alraune Zech**[2], **Gabriel C. Rau**[3], **and Peter Bayer**[1]

[1]Applied Geology, Institute of Geosciences and Geography, Martin Luther University Halle-Wittenberg, Halle, Germany, [2]Department of Earth Sciences, Utrecht University, Utrecht, The Netherlands, [3]School of Environmental and Life Sciences, The University of Newcastle, Callaghan, NSW, Australia

Key Points:

- We model advective heat transport through realizations of heterogeneous hydraulic conductivity to determine thermal retardation
- Increasing heterogeneity lead to a reduction in thermal retardation, a phenomenon we name "field-scale local thermal non-equilibrium (LTNE)"
- We propose a formula to approximate field-scale LTNE by estimating retardation as a function of log-conductivity variance and Péclet number

Supporting Information:

Supporting Information may be found in the online version of this article.

Correspondence to:

H. Gebhardt,
hannah.gebhardt@geo.uni-halle.de

Citation:

Gebhardt, H., Zech, A., Rau, G. C., & Bayer, P. (2025). Effective thermal retardation in aquifers of heterogeneous hydraulic conductivity. *Water Resources Research*, *61*, e2025WR040153. https://doi.org/10.1029/2025WR040153

Received 5 FEB 2025
Accepted 16 SEP 2025

Author Contributions:

Conceptualization: Hannah Gebhardt, Alraune Zech, Gabriel C. Rau, Peter Bayer
Formal analysis: Hannah Gebhardt
Funding acquisition: Peter Bayer
Methodology: Hannah Gebhardt, Alraune Zech, Gabriel C. Rau, Peter Bayer
Software: Hannah Gebhardt
Supervision: Gabriel C. Rau, Peter Bayer
Visualization: Hannah Gebhardt
Writing – original draft: Hannah Gebhardt
Writing – review & editing: Alraune Zech, Gabriel C. Rau, Peter Bayer

Abstract Thermal retardation and dispersion are important processes affecting advective heat transport in sedimentary aquifers, yet little is known how they are influenced by heterogeneity of hydraulic conductivity. We investigate the effect of macro-scale heterogeneity on transient heat transport in a three-dimensional domain through direct numerical Monte-Carlo simulations. The model describes the evolution of a heat plume in a heterogeneous aquifer generated by a borehole heat exchanger. We characterize the transport by calculating the dispersion coefficient and effective thermal retardation factor as ensemble average of the heterogeneous realizations. In addition to different degrees of heterogeneity, we examine the influence of the thermal Péclet number on the effective thermal retardation factor. Simulations reveal that for homogeneous hydraulic conductivity, the effective thermal retardation factor equals the predicted, apparent thermal retardation factor. However, in heterogeneous cases, the effective thermal retardation factor is substantially lower than the apparent value at early times, with this effect becoming more pronounced as the Péclet number increases. We attribute the deviation of the effective thermal retardation factor from the apparent value to preferential flow through zones with higher hydraulic conductivity and delayed local heat diffusion into zones with lower hydraulic conductivity. Assuming that the effective thermal retardation factor differs from the apparent value in the presence of local thermal non-equilibrium (LTNE) effects, we call the observed effect "field-scale LTNE." Finally, we derive a formula estimating effective thermal retardation as a function of log-conductivity variance and the Péclet number. Our results can improve heat tracer techniques in hydraulically heterogeneous environments.

1. Introduction

Quantifying advective heat transport in sedimentary aquifers is essential for process understanding and various applications, including the role of groundwater-sourced thermal refugia (e.g., KarisAllen et al., 2022; Kurylyk et al., 2014, 2015), heat tracing to estimate streambed fluxes (e.g., Anderson, 2005; Bertagnoli et al., 2024; Constantz, 2008; Halloran et al., 2016; Kurylyk et al., 2019; Rau et al., 2014; Shi, Zhan, et al., 2024), estimation of aquifer thermal and hydraulic properties (Colombani et al., 2015; Doro et al., 2015; Furlanetto et al., 2024; Klepikova et al., 2016; Ma et al., 2012; Sarris et al., 2018; Somogyvári & Bayer, 2017; Vandenbohede et al., 2009; Wagner et al., 2014; Wildemeersch et al., 2014) or the operation of shallow geothermal systems (Hähnlein et al., 2013; Pophillat et al., 2020). In this context, heterogeneous aquifers pose a particular challenge. The large variability of hydraulic conductivity (K) creates preferential flow pathways, non-uniform temperature fronts (Ferguson, 2007; Hoffmann et al., 2019; Irvine, Simmons, et al., 2015; Schornberg et al., 2010), and enhanced thermal dispersion (Chang & Yeh, 2012; Hidalgo et al., 2009).

Spreading of heat during advective transport in aquifers is caused by thermal diffusion (in the pore space and in the solid matrix) and thermal dispersion. The latter arises from both mechanical dispersion due to pore-scale velocity variations (Green et al., 1964; de Marsily, 1986) and differential advection at the macro-scale due to heterogeneous hydraulic conductivity (de Marsily, 1986; Sauty et al., 1982). However, the role of mechanical and macro-dispersion for heat transport in porous media remains elusive (e.g., Anderson, 2005; Baek et al., 2024; Park et al., 2015, 2018).

The effect of heterogeneity in hydraulic conductivity on solute dispersion has been thoroughly investigated by stochastic, field, and numerical methods (e.g., Dagan, 1989; Gelhar & Axness, 1983; Sudicky, 1986; Tompson & Gelhar, 1990). The meta-study on reliable field site macrodispersivities of Zech et al. (2015) confirmed

theoretical results: solute dispersion does not universally scale but increases with distance up to an asymptotic value, which is representative of different heterogeneities and is formation-specific.

While heat and solute transport are described by mathematically analogous equations, thermal diffusion is several orders of magnitude higher than molecular diffusion (Anderson, 2005) resulting in a smoothing effect of the temperature front compared to solute transport (Irvine, Simmons, et al., 2015). The relationship between dispersion and velocity in heat transport exhibits the same behavior as solute transport in the dispersion-dominant regime (Péclet number > 5), where dispersion increases linearly with velocity under pore-scale or laboratory-scale conditions (e.g., Baek et al., 2022, 2024; Rau et al., 2012). However, debate about the transferability of dispersion values between heat and solute transport is ongoing for field-scale problems.

Numerical studies have shown a strong influence of aquifer heterogeneity on thermal macrodispersion (Ferguson, 2007; Hidalgo et al., 2009; Molnár et al., 2025). Hidalgo et al. (2009) used a stochastic approach to investigate the effect of heterogeneous hydraulic conductivity on the steady-state heat plume generated by a line-like source in a three-dimensional domain. They found that transverse dispersion is proportional to the variance and correlation length of the log-conductivity (ln K) field. Similarly, through stochastic analysis of field-scale heat advection, Chang and Yeh (2012) revealed a linear relationship between macrodispersion coefficients (longitudinal and transverse) and variance in ln K. They conclude that, while the correlation length of ln K enhances heat advection at the field scale, the effective thermal conductivity reduces heat advection.

To compare heat and conservative solute transport in porous media, Vandenbohede et al. (2009) conducted two push-pull tests in a deep Tertiary aquifer in Belgium. They found a notable difference between longitudinal dispersion of heat and solute. While solute dispersivity increased with travel distance, thermal dispersivity did not exhibit a clear scale dependency. The authors attributed this difference to dissimilar position and shape of transition zones between injection and pristine water during solute and heat transport. Unlike solutes—which are transported solely through the pore water—heat propagates through both the fluid phase and the solid matrix of the porous medium. Tang and van der Zee (2022) incorporated a scale-dependent thermal macrodispersion relationship in their numerical models to investigate its effect on the recovery efficiency in aquifer thermal energy storage (ATES) systems.

Compared to solute transport, advective heat transport progresses more slowly because the heat capacity of the solid retards the thermal front. This delay is quantified by a thermal retardation factor that can be defined in two distinct ways: (a) the predicted, apparent thermal retardation factor R_{app}, which is related to the volumetric heat capacities of the aquifer and groundwater, and (b) the measured, effective thermal retardation factor R_{eff}, defined as the ratio of seepage velocity to thermal front velocity (Gossler et al., 2019). A standard approach in most studies of heat transport in porous aquifers is the assumption of local thermal equilibrium (LTE) between the solid and fluid phases (Gossler et al., 2020; Pastore et al., 2018; Rau et al., 2014; Roshan et al., 2014; Stauffer et al., 2014). This means that immediate temperature equilibrium between the solid and fluid phases is assumed, implying that there is sufficient time for heat to diffuse into the solid grains as the thermal front is transported by advection. This simplifies the two-phase nature of the porous medium by volume averaging, resulting in a single-phase heat transport equation (Whitaker, 1991).

Gossler et al. (2019) argued that when the LTE assumption holds, R_{app} and R_{eff} are expected to be of similar magnitude. However, experimental studies (Baek et al., 2022; Bandai et al., 2017; Gossler et al., 2019), as well as theoretical and numerical investigations (Gossler et al., 2020; Hamidi et al., 2019; Heinze & Hamidi, 2017; Roshan et al., 2014; Shi, Wang, et al., 2024), indicate that the LTE assumption may be violated under specific conditions common in natural systems. These include high flow velocities and preferential flow pathways, which are characteristic of coarse-grained materials. Under such conditions, the local thermal non-equilibrium (LTNE) approach, which employs separate energy balance equations for the solid and fluid temperature fields, provides a more accurate and realistic framework for describing heat transport (Sözen & Vafai, 1990). These coupled energy balance equations incorporate a heat transfer coefficient that depends on the solid-fluid interface area and must be determined experimentally (Kaviany, 1995). Levec and Carbonell (1985) presented experimental evidence of LTNE effects in ideal porous media demonstrating that the thermal front in the solid phase can lag behind the front in the fluid phase.

While R_{app} assumes LTE, R_{eff} is potentially affected by LTNE effects. Thus, deviations of R_{eff} from R_{app} indicate LTNE effects (Gossler et al., 2019). Recent studies have demonstrated that LTNE effects can influence estimates

of thermal retardation and dispersion in natural sediments under Darcian flow conditions (Baek et al., 2022; Gossler et al., 2019, 2020; Roshan et al., 2014; Shi, Wang, et al., 2024). In column sand experiments, Bandai et al. (2017) and Gossler et al. (2019) showed that effective thermal dispersion depends on particle size, whereas solute dispersion does not, attributing this difference to LTNE effects. Similarly, Pastore et al. (2018) observed non-uniform flow and channeling during flow through sediments and suggested that coarser material likely promotes LTNE conditions. Flow velocity and the solid grain size have been found to strongly impact LTNE effects (Baek et al., 2022; Gossler et al., 2019, 2020; Shi, Wang, et al., 2024). Similar effects have been observed for heat transport during water infiltration into partially saturated soil (Heinze & Blöcher, 2019).

So far, most studies on LTNE effects have focused on small-scale setups, that is, pore-scale or laboratory-scale homogeneous media (Baek et al., 2022; Gossler et al., 2019, 2020; Roshan et al., 2014; Shi, Wang, et al., 2024). Upscaling techniques to extend small-scale findings of LTNE effects to the field-scale are lacking (Heinze, 2024). Hamidi et al. (2019) examined the impact of hydraulic heterogeneity on temperature differences between LTE and LTNE models in a synthetic geothermal system. Their findings indicate that, over 40 years, the temperature of the produced water diverges by approx. 4% between LTE and LTNE models. However, field observations with geothermal groundwater use or heat tracer tests do not offer a unique picture of the concerted effect of macro-dispersion as well as channelized flow causing LTNE (Klepikova et al., 2016; Somogyvári & Bayer, 2017; Vandenbohede et al., 2009; Wagner et al., 2014). Inconsistencies arising from LTE assumptions may be masked by dispersion effects when interpreting temperature measurements in groundwater systems.

Despite the growing understanding of LTNE at the pore scale, the implications of large-scale heterogeneity on thermal non-equilibrium remain poorly understood. We address this knowledge gap through a systematic investigation of the relationship between heterogeneous hydraulic conductivity and LTNE effects. We pay particular attention to distinguish between delayed local diffusion induced by LTNE effects and thermal retardation, and dispersion driven by differential advection. For this purpose, we develop a stochastic heterogeneous hydraulic conductivity model framework simulating the transient evolution of a 3D heat plume originating from a line-like heat source. We analyze spatial moments and the thermal breakthrough curve (BTC) of the resulting heat plumes stochastically to derive estimates of retardation and dispersion. Our results lead to the development of an equation to estimate the effective thermal retardation factor as a function of hydraulic conductivity variance and the thermal Péclet number.

2. Methods

2.1. Governing Equations

We consider steady-state flow and transient heat transport based on the assumption of an LTE at the pore scale, that is, instantaneous heat transfer between phases. Density and viscosity of water are considered to be constant. Groundwater flow follows Darcy's law. Heat transport is governed by the advection-diffusion equation:

$$\nabla \cdot \mathbf{q}(\mathbf{r}) = \nabla \cdot [-K(\mathbf{r})\nabla h(\mathbf{r})] = 0, \tag{1}$$

$$\rho_b c_b \frac{\partial T(\mathbf{r})}{\partial t} = \lambda_b \nabla^2 T(\mathbf{r}) - \rho_f c_f \mathbf{q}(\mathbf{r}) \cdot \nabla T(\mathbf{r}) + P_t(\mathbf{r}), \tag{2}$$

where $\mathbf{r} = (x, y, z)$ (m) is the coordinate vector, $\mathbf{q}(\mathbf{r}) = -K(\mathbf{r})\,\nabla h(\mathbf{r})$ is the Darcy velocity, K (m/s) is hydraulic conductivity, h (m) is piezometric head, T (K) is temperature, t (s) is time, P_t (J/m^3 s) is the thermal production term, ρ_f (kg/m^3) is the density of water, c_f (J/kg K) is the specific heat capacity of water, $\rho_f c_f$ (J/m^3 K) is the volumetric heat capacity of groundwater, λ_b (J/m s K) is the bulk thermal conductivity and $\rho_b c_b$ (J/m^3 K) is the bulk volumetric heat capacity, which are expressed as arithmetic means of the solid and fluid phase:

$$\rho_b c_b = n\rho_f c_f + (1-n)\rho_s c_s, \tag{3}$$

$$\lambda_b = n\lambda_f + (1-n)\lambda_s, \tag{4}$$

where n is porosity, $\rho_s c_s$ (J/m^3 K) is the solid volumetric heat capacity. λ_f and λ_s (J/m s K) are the thermal conductivity of water and the solid phase, respectively.

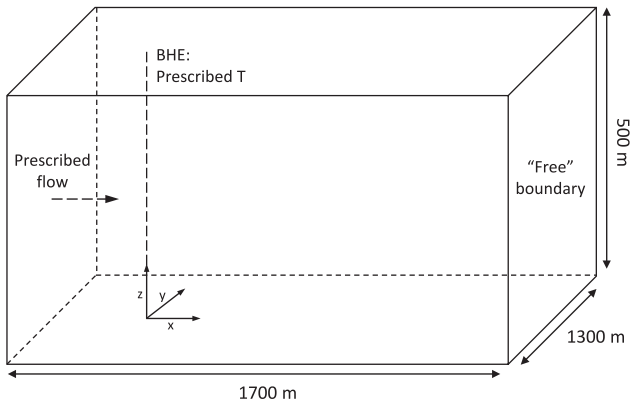

Figure 1. 3D numerical model setup with a line heat source representing a borehole heat exchanger at prescribed temperature T. A prescribed flow boundary condition is applied on the entire $x = -200$ m plane (left boundary). The right boundary at $x = 1,500$ m is an outflow boundary allowing water and heat energy to exit freely. Other boundaries are specified as no-flow and adiabatic.

The dimensionless thermal Péclet number Pe characterizes the heat transport problem by relating the relative contributions of heat flux by advection and by conduction (e.g., de Marsily, 1986):

$$Pe = \frac{\rho_f c_f q_0 L}{\lambda_b}, \tag{5}$$

where L (m) is a characteristic length and q_0 (m/s) is the mean flow velocity aligned with the x-direction.

The dimensionless thermal retardation factor characterizes the lag of the thermal front relative to fluid velocity caused by heat diffusion. To identify effects of LTNE, we determine both the apparent thermal retardation factor R_{app} and the effective thermal retardation factor R_{eff} through:

$$R_{\text{app}} = \frac{\rho_b c_b}{n \rho_f c_f}, \tag{6}$$

$$R_{\text{eff}} = \frac{v_a}{v_t}, \tag{7}$$

where $v_a = q_0/n_{\text{eff}}$ (m/s) is the seepage velocity with n_{eff} being the effective porosity (−). $v_t = q_0/n_{\text{eff}} R_{\text{eff}}$ (m/s) is the thermal front velocity. While R_{app} is predicted from aquifer and hydraulic properties, R_{eff} is measured from plume extensions.

2.2. Numerical Model

The equations governing transient heat transport, based on the assumption of pore-scale LTE (Equations 1 and 2), are solved using the *Multiphysics Object-Oriented Simulation Environment* (MOOSE), an open-source, parallel finite element numerical modeling framework (Gaston et al., 2009; Permann et al., 2020). MOOSE includes the *PorousFlow* library, which enables the simulation of transport and flow in porous media (Wilkins et al., 2020, 2021). As shown by Bastías Espejo et al. (2021), MOOSE also supports the simulation of spatially heterogeneous systems.

We simulate a heat plume in a rectangular domain of size 1,700 m × 1,300 m × 500 m (Figure 1). The numerical setup is similar to the one described by Hidalgo et al. (2009). The model domain is spatially discretized by 183,300 hexahedral elements with a grid element size of $\Delta x = \Delta y = \Delta z = 20$ m. Flow is prescribed at the inflow boundary, which is located at the $x = -200$ m plane. At the outflow boundary located at the $x = 1,500$ m plane, water is removed at exactly the rate specified by the Darcy equation. The remaining boundaries, parallel to the mean flow direction, are impermeable.

Heat is generated by a borehole heat exchanger (BHE) as a vertically extended line-like source of constant temperature. It provides a continuous heat input of 20 K above the initial temperature. It is positioned at the origin of the coordinate system. The interested reader can find details on the mathematical specification of flow and heat transport boundary and initial conditions as well as on the domain and temporal discretization in Supporting Information S1.

Thermal and hydraulic parameters representative of a clean sand were selected and are listed in Table 1. The bulk thermal conductivity was adopted from Hidalgo et al. (2009) to ensure comparability with their results. The specific heat capacity of the solid, although slightly higher than that of quartz, follows Hecht-Méndez et al. (2010), who used the same value for modeling a comparable sand aquifer. The density of the solid corresponds to that of quartz (Schön, 1996). Both the bulk thermal conductivity and the bulk thermal volumetric heat capacity fall within ranges reported for saturated sand (Stauffer et al., 2014). All except for hydraulic conductivity are considered homogeneous and are maintained as constants across all simulations.

Several studies have shown that in advection-dominated systems, heat transport is strongly controlled by variations in hydraulic conductivity, whereas porosity exerts a lesser influence and thermal properties are least

Table 1
Parameter Values Assigned to the Numerical Model

Parameter	Symbol	Value	Unit	Comment/Source
Effective porosity	n_{eff}	0.25	–	Freeze and Cherry (1979)
Volumetric heat capacity of water	$\rho_f c_f$	4.18×10^6	J/m^3 K	Haynes et al. (2016)
Specific heat capacity of the solid	c_s	880	J/kg K	Hecht-Méndez et al. (2010)
Density of the solid	ρ_s	2,650	kg/m^3	Quartz density (Schön, 1996)
Bulk volumetric heat capacity	$\rho_b c_b$	2.79×10^6	J/m^3 K	Equation 3
Bulk thermal conductivity	λ_b	1.6369	J/m s K	Hidalgo et al. (2009)
Apparent thermal retardation factor	R_{app}	2.67	–	Equation 6

sensitive (e.g., Hoffmann et al., 2019; Klepikova et al., 2016; Ma et al., 2012; Rau et al., 2014; Wagner et al., 2014). This aligns with literature findings showing that both thermal conductivity and porosity vary over much narrower ranges than hydraulic conductivity: while K can span 3–4 orders of magnitude over short distances, porosity in unconsolidated deposits ranges between 0.25 and 0.7 (Freeze & Cherry, 1979), and the thermal conductivity of saturated sediments generally varies between 1.4 and 2.2 W/m K (Anderson, 2005).

Following a standard practice in stochastic hydrogeology, hydraulic conductivity is modeled as a random space function, reflecting its erratic spatial variability and the uncertainty associated with limited site characterization (Dagan, 1986; Gelhar, 1986). Most studies assume spatially variable K and homogeneous porosity, since porosity variability is generally considered secondary (Amiri et al., 2023; Libera et al., 2019). This approach has also been adopted in heat transport studies (e.g., Ferguson, 2007; Irvine, Simmons, et al., 2015; Molnár et al., 2025; Sommer et al., 2013), enabling controlled examination of the dominant influence of K heterogeneity.

2.3. Simulation Scenarios

We study the effects of heterogeneity on macro-scale heat transport using spatial random fields for the hydraulic conductivity distribution $K(\mathbf{r})$ during the simulations. The heterogeneous hydraulic conductivity field follows a log-normal distribution $f(\mathbf{r}) = \ln K(\mathbf{r})$, that is, the log-transformed hydraulic conductivity is characterized by its mean and variance. The spatial correlation is represented by a Gaussian covariance model. It is fully characterized by the semi-variogram based on the correlation length L in each spatial direction. Typically, correlation lengths in horizontal directions are assumed equal ($L_x = L_y$) while the vertical correlation length L_z is considered much smaller due to sedimentary layering. It is usually characterized through the anisotropy ratio of $e = L_z/L_x$.

We generate random heterogeneous hydraulic conductivity fields (Figure 2) using the Python package GSTools (Müller et al., 2022). The geometric mean of the hydraulic conductivity is set to 4.1×10^{-5} m/s, which is in the range of clean sand (Freeze & Cherry, 1979). We test variances for ln K of $\sigma^2_{\ln K} = 1, 2$ and 3 and examine the effect of three characteristic correlation lengths in horizontal directions of $L_{x,1} = 100$ m, $L_{x,2} = 125$ m and $L_{x,3} = 150$ m ($L_y = L_x$). We keep the vertical correlation length constant at $L_z = 50$ m. We create ensembles of heterogeneous ln K-fields for the various combinations of $\sigma^2_{\ln K}$ and L_x. Each ensemble is comprised of 100 realizations.

Besides studying the effect of strength of hydraulic conductivity heterogeneity (i.e., $\sigma^2_{\ln K}$), we investigate the influence of Darcy velocity and correlation length L_x on effective thermal retardation. Therefore, we define five simulation scenarios with varying Péclet numbers (Table 2). Scenario *L1q2*, with $Pe = 14.94$, is selected as the base case and uses the median Darcy velocity and the smallest correlation length. The full set of scenarios spans thermal Péclet numbers from 4.98 to 25.03, where $Pe \approx 5$ represents the lower boundary of the advection-dominant regime. The other scenarios are designed as targeted variations of the base case: scenarios *L1q1* and *L1q3* vary the Darcy velocity while keeping the correlation length constant, and scenarios *L2q2* and *L3q2* vary the correlation length while keeping the Darcy velocity constant.

In a stochastic framework, different averaging strategies yield different plume characteristics. Here, we focus on the heat plume evolution based on *effective* ensemble averages. We determine effective thermal dispersion and thermal velocity by first calculating these quantities for each realization, and then we average over all realizations. This approach contrasts with the use of *ensemble* quantities, which are derived from the ensemble averaged

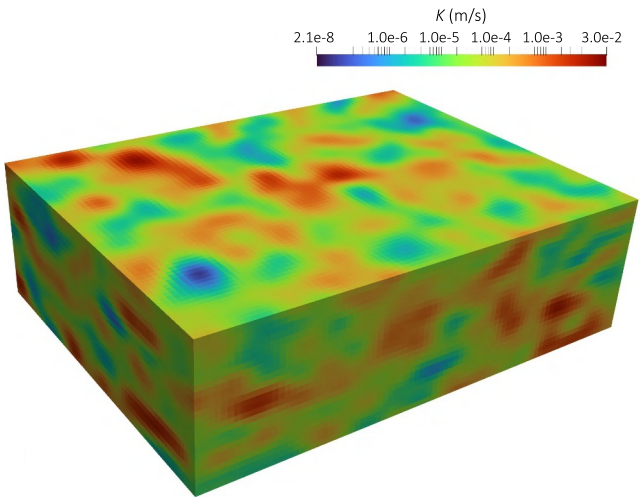

Figure 2. An example of a heterogeneous realization of the hydraulic conductivity (K) fields for $\sigma^2_{\ln K} = 3$ as was used to model flow and heat transport.

temperature distribution and thus take into account an artificial spreading caused by fluctuations of the plume center of mass positions from realization to realization. The effective quantities better reflect the flow and spreading behavior in a single aquifer (Kitanidis, 1988). However, the difference between the effective and ensemble quantities vanishes for infinite times or with distance from the heat source, respectively, due to ergodicity (Attinger et al., 1999; Dagan, 1990; Dentz et al., 2000).

2.4. Spatial Moment Analysis

We determine thermal velocity and the transverse thermal dispersion from spatial moment analysis of the simulated temperature distribution $T(x, y, z, t)$. The zeroth moment $\mu^{(0)}(t) = \int T(\mathbf{r}, t)\, \mathrm{d}\mathbf{r}$ (with $\mathbf{r} = (x, y, z)$) is a measure for the stored thermal energy.

The first spatial moments characterize the position of the thermal plume center of mass. We determine the first spatial moment in main flow direction x:

$$\mu_x^{(1)}(t) = \int_z \int_y \int_x x \cdot T(x, y, z, t)\, \mathrm{d}x\, \mathrm{d}y\, \mathrm{d}x. \tag{8}$$

We can calculate the thermal velocity of each realization v_t as change of the normalized center of mass position. This results in a time-dependent thermal velocity:

$$v_t(t) = \frac{\mathrm{d}\mu_x^{(1)}(t)}{\mathrm{d}t} \cdot \frac{1}{\mu^{(0)}(t)}. \tag{9}$$

We compute $v_t(t)$ for each realization, perform the ensemble average (denoted with $\langle\cdot\rangle$) and determine the time-dependent effective thermal retardation factor from Equation 7 (e.g., Burr et al., 1994; Rajaram, 1997):

$$R_{\mathrm{eff}}(t) = \frac{v_a}{\langle v_t(t)\rangle}. \tag{10}$$

In addition, we study the transverse dispersion for the steady-state temperature distribution $T(x, y, z, t = \infty)$. We calculate the second moment in the transverse horizontal direction while retaining the spatial dependency in the flow direction, as follows:

$$\mu_{yy}^{(2)}(x) = \int_z \int_y y^2 \cdot T(x, y, z, t = \infty)\, \mathrm{d}y\, \mathrm{d}z. \tag{11}$$

The steady-state transverse plume extent $\kappa_{yy}(x)$ follows as the second centered moment of the normalized temperature distribution $\kappa_{yy}(x) = \frac{\mu_{yy}^{(2)}(x)}{\mu^{(0)}} - \left[\frac{\mu_y^{(1)}}{\mu^{(0)}}\right]^2$. Note that we compute the second moment for every z-coordinate and then average vertically. This approach reflects analysis of point measurements instead of two-dimensional (depth averaged) measurement, where the temperature field would first be averaged along the z-direction before computing the spatial moments. The spatial moments are obtained through numerical integration along the nodes using the composite trapezoidal rule, which involves applying the trapezoidal rule to each subinterval and summing the resulting values.

Again, we calculate $\kappa_{yy}(x)$ for each realization and perform the ensemble average to obtain the *effective* steady-state transverse plume extent:

Table 2
Simulation Scenarios Corresponding to Various Values of Characteristic Length and Darcy Velocity

Scenario	Characteristic length	Darcy velocity	Pe
L1q2	$L_{x,1} = L_{y,1} = 100$ m	$q_{0,2} = 5.85 \times 10^{-8}$ m/s	14.94
L1q1	$L_{x,1} = L_{y,1} = 100$ m	$q_{0,1} = 1.95 \times 10^{-8}$ m/s	4.98
L1q3	$L_{x,1} = L_{y,1} = 100$ m	$q_{0,3} = 9.80 \times 10^{-8}$ m/s	25.03
L2q2	$L_{x,2} = L_{y,2} = 125$ m	$q_{0,2} = 5.85 \times 10^{-8}$ m/s	18.67
L3q2	$L_{x,3} = L_{y,3} = 150$ m	$q_{0,2} = 5.85 \times 10^{-8}$ m/s	22.41

$$\kappa_{yy}^{\text{eff}}(x) = \langle \kappa_{yy}(x) \rangle. \tag{12}$$

The effective transverse dispersion coefficient D_T^{eff} (m^2/s) is calculated as the rate of increase of the effective steady-state transverse plume extent $\kappa_{yy}^{\text{eff}}(x)$ along the mean flow direction (Hidalgo et al., 2009):

$$D_T^{\text{eff}} = \frac{1}{2} \frac{\text{d}\kappa_{yy}^{\text{eff}}(x)}{\text{d}x} q_0. \tag{13}$$

The time derivative of the first longitudinal moment (Equation 9) and the transverse dispersion coefficient (Equation 13) are obtained through central finite differences at the interior points and forward/backward differences at the boundaries.

To identify the part of the effective transverse dispersion coefficient D_T^{eff} that is caused by the heterogeneous structure of the hydraulic conductivity, we make use of the well-established concept from solute transport, that macrodispersion is composed of a diffusive and a dispersive part (Hidalgo et al., 2009):

$$D_T = D_{\text{diff}}^{\text{SS}} + \alpha_T q_0 = \frac{\lambda_b}{\rho_f c_f} + \alpha_T q_0, \tag{14}$$

where $D_{\text{diff}}^{\text{SS}} = \frac{\lambda_b}{\rho_f c_f}$ is the contribution from thermal conductivity in steady-state.

The transverse macrodispersivity α_T (m) represents the contribution of heat plume spreading in transverse horizontal direction caused by aquifer heterogeneity. We determined α_T for all heterogeneous ensembles from the ensemble's effective transverse dispersion coefficient D_T^{eff} using Equation 14. Note that $\alpha_T = 0$ for the homogeneous case and consequently $D_T/D_{\text{diff}}^{\text{SS}} = 1$. We will use the latter as reference to identify the increase of transverse dispersion by heterogeneity.

2.5. BTC Analysis

As we analyze the longitudinal spreading behavior of the plume spatially dependent, we determine longitudinal dispersion coefficients D_L (m^2/s) from BTC analysis following a common procedure in solute transport analysis.

We fit the BTCs of each simulated temperature distribution to the analytical solution of van Genuchten and Alves (1982) for Equations 1 and 2 under the transport situation of a step input as specified in Section 2.2. The equation and details of the fitting procedure are provided in Supporting Information S1.

The normalized numerical BTC at the transverse plume center of mass of each realization $T(x,t)$ are fitted to the normalized analytical solution. This is done for each distance x from the heat source at each depth z. Figure S8 in Supporting Information S1 demonstrates that the analytical solution provides a good fit across different distances and degrees of heterogeneity. We then take the depth average which results in a distance dependent macrodispersion coefficient $D_L(x)$. The estimated longitudinal macrodispersion coefficients of all realizations are ensemble averaged to achieve the effective longitudinal macrodispersion coefficient $D_L^{\text{eff}}(x) = \langle D_L(x) \rangle$.

As with transverse dispersion, we identify the part of the effective longitudinal dispersion coefficient D_L^{eff} that is caused by the heterogeneous structure of the hydraulic conductivity splitting it off into a diffusive and a dispersive part (de Marsily, 1986):

$$D_L = D_{\text{diff}} + D_{L,\text{disp}} = \frac{\lambda_b}{\rho_b c_b} + \alpha_L \left| \frac{\rho_f c_f}{\rho_b c_b} q \right|, \tag{15}$$

where D_{diff} represents the bulk thermal diffusivity of the saturated medium, $D_{\text{L,disp}}$ is the dispersive component arising from spatial heterogeneity, and α_L (m) is the longitudinal macrodispersivity. Mechanical dispersion effects due to pore-scale velocity fluctuations are neglected in this study. Note that the specifications of the diffusive and dispersive components differ in Equations 14 and 15 since we study D_L under transient conditions.

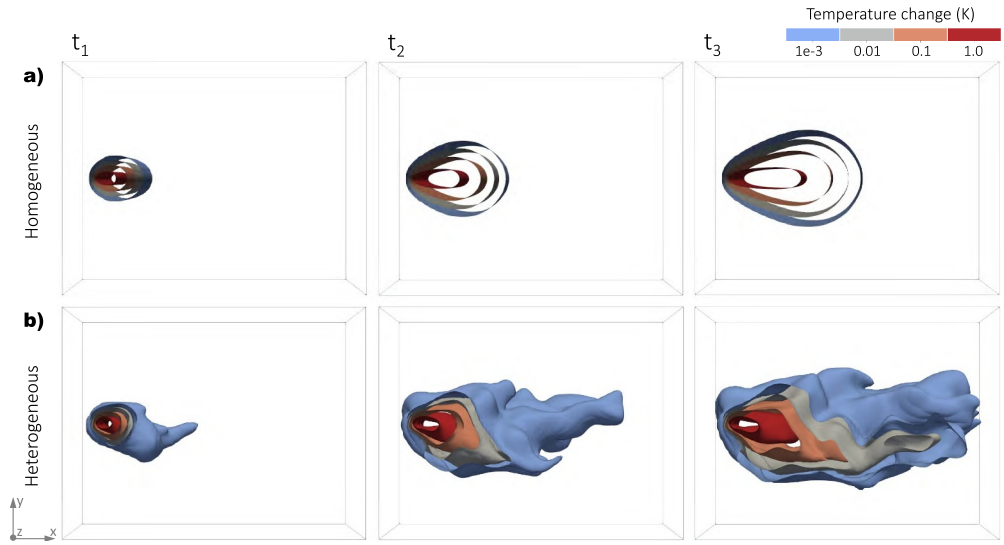

Figure 3. Temperature evolution for (a) the homogeneous case, and (b) a heterogeneous realization with $\sigma^2_{\ln K} = 3$ (from *L1q2*, Table 2) at times $t_1 = 1 \times 10^9$ s, $t_2 = 3 \times 10^9$ s and $t_3 = 5 \times 10^9$ s.

Just as for α_T, α_L reflects the longitudinal spreading caused by aquifer heterogeneity. Consequently, for the homogeneous case $D_L = D_{\text{diff}}$. We determined α_L for all heterogeneous ensembles from the ensemble's effective longitudinal dispersion coefficient D_L^{eff} using Equation 15.

Using stochastic analysis of thermal transport, Chang and Yeh (2012) demonstrated for isotropic conditions that longitudinal thermal macrodispersivity increases monotonically with time until reaching its asymptotic value, consistent with results for conservative transport (Dagan, 1989; Gelhar et al., 1992). The asymptotic values can be calculated as a function of the log-conductivity variance $\sigma^2_{\ln K}$ according to Chang and Yeh (2012) (Equations 5 and 6 in Supporting Information S1).

3. Results

3.1. Heat Plume Evolution

The propagation of the heat plume generated by the BHE differs notably between homogeneous and heterogeneous hydraulic conductivity at early times, that is, well before steady-state is reached (Figure 3). Heat transport in a domain with homogeneous hydraulic conductivity shows the familiar uniform plume shape (Figure 3a). In contrast, for a single heterogeneous realization with a log-conductivity variance of $\sigma^2_{\ln K} = 3$ (Figure 3b), spatial variations in hydraulic conductivity create a non-uniform flow field leading to preferential heat transport and zones of delayed warming. In addition, the longitudinal extent of the heat plume is almost double in size compared to the homogeneous case.

3.2. Transverse Thermal Dispersion

Heterogeneity increases the transverse thermal dispersion at steady-state, as indicated by the wider transverse heat plume extents and larger transverse dispersion coefficients shown in Figure 4. Displayed are the effective transverse second centered moment $\kappa^{\text{eff}}_{yy}(x)$ (Equation 12) in Figure 4a and the transverse dispersion coefficient normalized by thermal diffusion $D_T/D^{\text{SS}}_{\text{diff}}$ (Equation 14) in Figure 4b, both as a function of the distance from the heat source for $Pe = 14.94$. Similar figures for other scenarios with $Pe = 4.98$ and $Pe = 25.03$ can be found in Supporting Information S1, Figures S2 and S3.

Higher log-conductivity variances result in a stronger increase in the lateral plume extent, $\kappa^{\text{eff}}_{yy}(x)$, indicating enhanced lateral spreading with distance from the heat source (Figure 4a). In contrast to Hidalgo et al. (2009), we did not observe boundary effects on the lateral plume extent (see Supporting Information S1), indicating that our domain size is of sufficient extent.

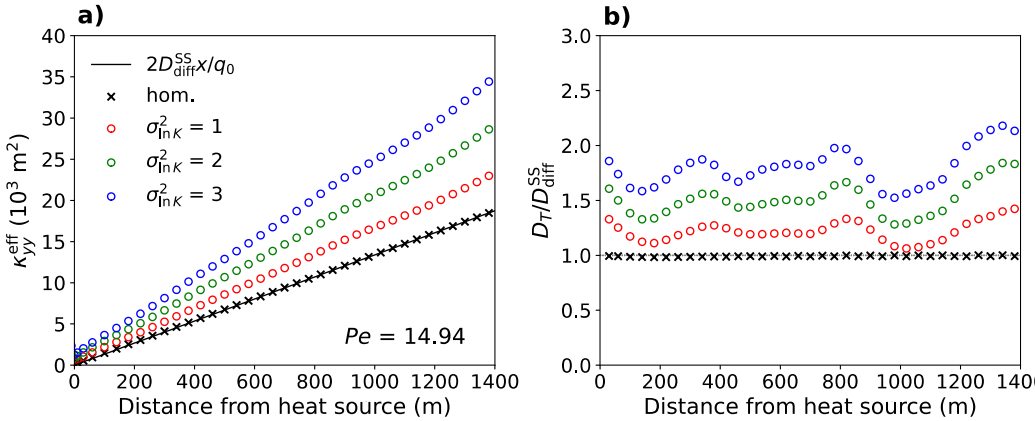

Figure 4. Steady-state transverse plume spreading: (a) second centered moment $\kappa^{\text{eff}}_{yy}(x)$ and (b) ratio of transverse dispersion coefficient and thermal diffusion; for different log-conductivity values $\sigma^2_{\ln K}$ (scenario *L1q2*, Table 2).

The spatial derivative of $\kappa^{\text{eff}}_{yy}(x)$, shown in Figure 4b, highlights the increase of the transverse dispersion coefficient D_T with increasing log-conductivity variance. D_T has almost doubled for $\sigma^2_{\ln K} = 3$ compared to the homogeneous case. We found that a higher thermal Péclet number also results in greater transverse dispersion coefficients (visualized in Figure S3 in Supporting Information S1). For small *Pe*, diffusion dominates, but dispersion increases with *Pe* as advection becomes dominant. As shown in Figure S3 in Supporting Information S1, the transverse dispersion coefficient D_T increases with both $\sigma^2_{\ln K}$ and *Pe*. When averaged along the distance from the heat source, D_T remains constant in the homogeneous case ($\sigma^2_{\ln K} = 0$) at 3.9×10^{-7} m^2/s for all *Pe*, corresponding to a normalized value $\left(D_T/D^{\text{SS}}_{\text{diff}}\right)$ of 1.0. In contrast, for $\sigma^2_{\ln K} = 1$, the average normalized transverse dispersion increases from approximately 1.1 to 1.3 (i.e., 4.2×10^{-7} to 5.1×10^{-7} m^2/s) as *Pe* increases from 4.98 to 25.03. For $\sigma^2_{\ln K} = 3$, the average normalized values increase more markedly, from about 1.3 (5.1×10^{-7} m^2/s) to 2.0 (7.9×10^{-7} m^2/s) over the same range of *Pe*. These trends reflect the growing influence of heterogeneity-driven dispersion under more advective conditions.

3.3. Longitudinal Thermal Dispersion

The scale-dependent effective longitudinal dispersion coefficient $D_L(x)$ (Equation 15) obtained from BTC fitting for three ensembles of increasing heterogeneity (from *L1q2*, Table 2) reveals that an increase of $\sigma^2_{\ln K}$ leads to a faster growth of D_L with distance from the heat source (Figure 5). In addition, an increase of $\sigma^2_{\ln K}$ leads to higher asymptotic values. We also see that a longer travel distance is required to reach asymptotic macrodispersion (Chang & Yeh, 2012) with increasing $\sigma^2_{\ln K}$. Generally, we observe a very good agreement between the theoretical asymptotic dispersions and values obtained from direct simulations far from the heat source. However, the asymptotic value has not been reached for the ensembles with $\sigma^2_{\ln K} > 1$. This is due to the limited domain size, extending only 15 correlation lengths from the heat source as larger variances require longer times/distances to reach the asymptotic value. These results are confirmed by Figure S4 in Supporting Information S1 showing the temporal evolution of the longitudinal plume extent $\kappa^{\text{eff}}_{xx}(t)$. As heterogeneity increases, $\kappa^{\text{eff}}_{xx}(t)$ reaches a higher asymptotic value while requiring more time to reach steady-state.

3.4. Effective Thermal Retardation

The time-dependent thermal velocity $v_t(t)$ and effective thermal retardation factor R_{eff} for scenario *L1q2* (Table 2) exhibit characteristic temporal trends that vary with the degree of heterogeneity (Figure 6). The thermal velocity was determined as ensemble mean using Equation 9 for the three values of $\sigma^2_{\ln K}$ and for the homogeneous case. Effective thermal retardation follows as the reciprocal of $v_t(t)$ multiplied with the constant seepage velocity v_a (Equation 10).

Thermal velocity shows a short initial increase before decreasing monotonically for all log-conductivity variances (Figure 6a). The higher the variance, the larger the thermal velocity, but also the faster the decrease. This is in

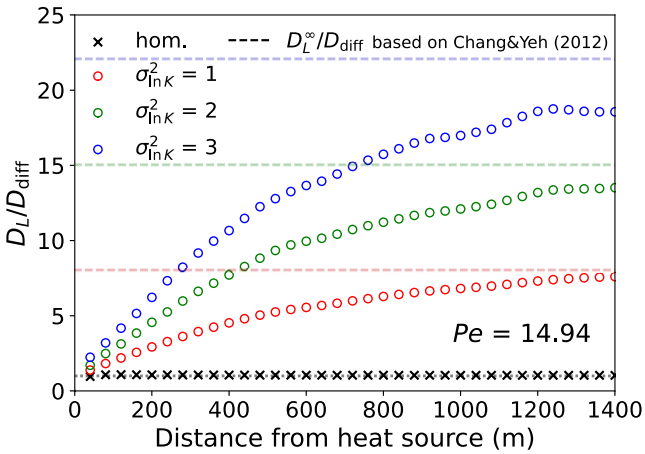

Figure 5. Scale-dependent longitudinal dispersion coefficient $D_L(x)$ normalized by bulk thermal diffusivity D_{diff} for different log-conductivity values $\sigma^2_{\ln K}$ (scenario *L1q2*, Table 2). The colored dashed lines indicate the asymptotic values for each $\sigma^2_{\ln K}$.

sharp contrast to the constant plume velocity for the homogeneous case. $v_t(t)$ approaches zero over time as the plume's center of mass changes progressively less and eventually reaches steady-state. Also, the 95% confidence intervals become smaller over time showing that all realizations follow the same temporal pattern. The largest velocity differences occur at the beginning of the transport process when local heterogeneity has the strongest impact.

The apparent thermal retardation R_{app}, being 2.67 for the parameters in Table 1, aligns perfectly with R_{eff} calculated for the homogeneous simulation for times far from steady-state (Figure 6b). As for thermal velocity, the behavior in heterogeneous fields deviates notably. R_{eff} is substantially lower than R_{app} at early times, increases monotonically and eventually exceeds R_{app}. The rate of increase grows with $\sigma^2_{\ln K}$. This indicates that the plume centroid is less retarded early in the transport but undergoes progressively greater retardation over time compared to the homogeneous case. We associate this effect with preferential flow through highly permeable areas, alongside delayed local heat diffusion into hydraulically less permeable zones, also visible in Figure 3b for a single heterogeneous realization.

The influence of the thermal Péclet number on the effective thermal retardation factor was examined by varying the Darcy velocity q_0 while keeping the correlation length constant (scenarios *L1q1*, *L1q2*, and *L1q3* in Table 2). We find that R_{eff} decreases at early times with increasing Darcy velocity (Figure 7), that is, increasing *Pe*. We link that to a more intensive preferential flow (similar to the effect of increasing heterogeneity), leading to more delay by local heat diffusion into hydraulically less permeable zones. The same effect is observed with increasing *Pe* by higher correlation length values L_x and constant Darcy velocity (Figure S6 in Supporting Information S1), but less pronounced.

3.5. Field-Scale LTNE and Macrodispersion

The differences between apparent thermal retardation R_{app} (reflecting pore-scale LTE conditions) and the effective retardation R_{eff} (potentially influenced by pore-scale LTNE), observed in our heterogeneous flow field simulations, strongly indicate the presence of LTNE effects on the field scale, even though we did not account for pore-scale LTNE effects. Motivated by the definition of macrodispersion, which captures spreading as a result of fluid velocity variations at the macro-scale due to heterogeneous hydraulic conductivity (de Marsily, 1986; Sauty et al., 1982), we describe the heterogeneity-induced initial increase in thermal velocity under transient conditions with the term *field-scale LTNE*.

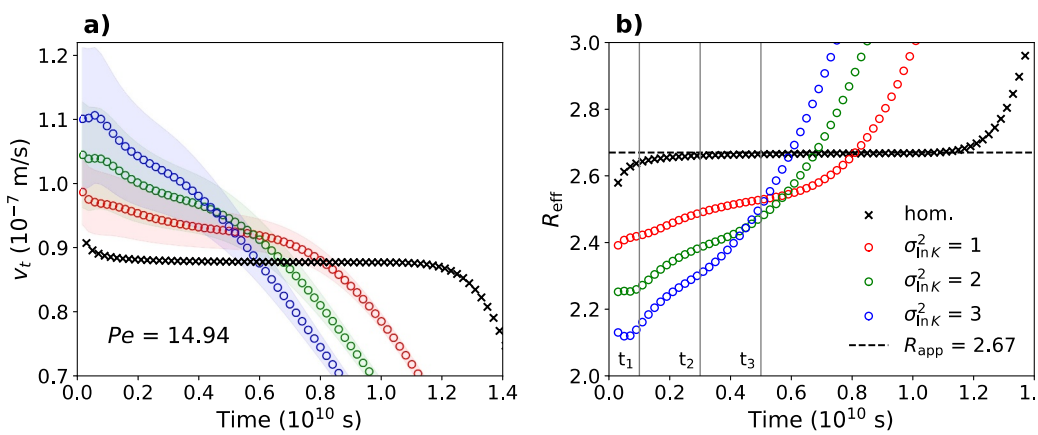

Figure 6. Temporal evolution of (a) thermal velocity and (b) effective thermal retardation for different values of log-conductivity $\sigma^2_{\ln K}$ (scenario *L1q2*, Table 2). The shaded areas in (a) represent the 95% confidence intervals of the thermal velocity. The dashed line in (b) indicates the value of the apparent thermal retardation factor R_{app} (Equation 6), the gray vertical lines are the three times shown in Figure 3.

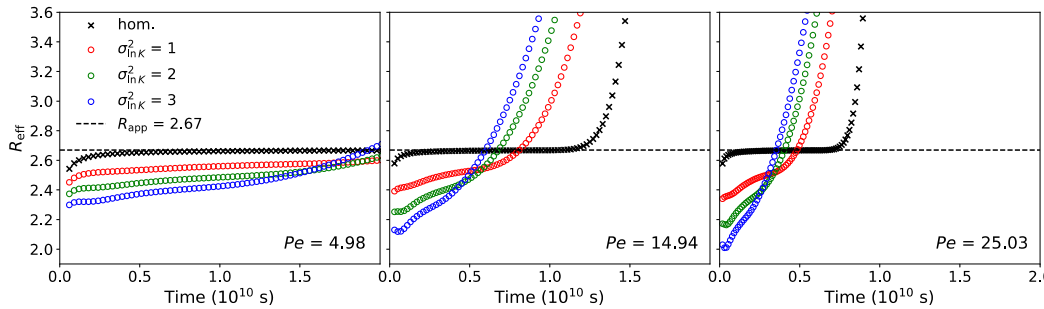

Figure 7. Effective thermal retardation evolution for three Darcy velocities (scenario *L1q1–L1q3*, Table 2) and three values of $\sigma^2_{\ln K}$. The correlation length is constant $L_x = 100$ m for all cases. The dashed line indicates the value of the apparent thermal retardation factor R_{app}.

To differentiate the effect of field-scale LTNE (associated with the time derivative of the first moment) from macrodispersion (related to the second spatial moment), we conducted simulations with homogeneous hydraulic conductivity and values of macrodispersion reflecting those of the heterogeneous ensembles. Specifically, we use the values of D_T as displayed in Figure 4b and D_L as displayed in Figure 5 for homogeneous simulations. For D_T we use constant values, resulting from the average over x. For longitudinal dispersion, we run simulations with a spatially increasing $D_L(x)$ (Figure 5). Note that transverse and longitudinal second centered moments of the heterogeneous case and the homogeneous case with macrodispersion are in good agreement (Figure S5 in Supporting Information S1), although the latter exhibits greater longitudinal plume extents during later times before steady-state is reached (Figure S5b in Supporting Information S1). More details on the implementation are provided in Supporting Information S1. Resulting effective retardation factors are shown in Figure 8.

Substantial differences arise in the effective thermal retardation factors for the homogeneous cases with macrodispersion, from both the homogeneous case without macrodispersion and from the heterogeneous case with the same macrodispersion (Figure 8). These differences become more pronounced as log-conductivity variance (and so macrodispersion) increases. Increasing the effective thermal dispersion coefficient for the homogeneous case leads to deviations of R_{eff} from R_{app}, indicating that the thermal velocity in the homogeneous case with macrodispersion is higher than in the homogeneous case without macrodispersion. The thermal velocity accelerates because the effective dispersion coefficient, which combines thermal diffusivity and advection-induced thermal dispersion, is treated as a single term in the advection-dispersion equation, without distinguishing between the diffusive and dispersive part. While the diffusive part of the effective dispersion coefficient affects thermal velocity, the dispersive component governs heat plume spreading. Consequently, increasing the effective dispersion coefficient to represent heterogeneity-induced macrodispersion enhances both thermal velocity and plume spreading.

Furthermore, we find that longitudinal macrodispersivity α_L is the primary driver for the increase in thermal velocity due to an increase in effective thermal dispersion, whereas the influence of the transverse macrodispersivity α_T on thermal velocity is marginal. At the same time, field-scale LTNE effects cannot be reproduced

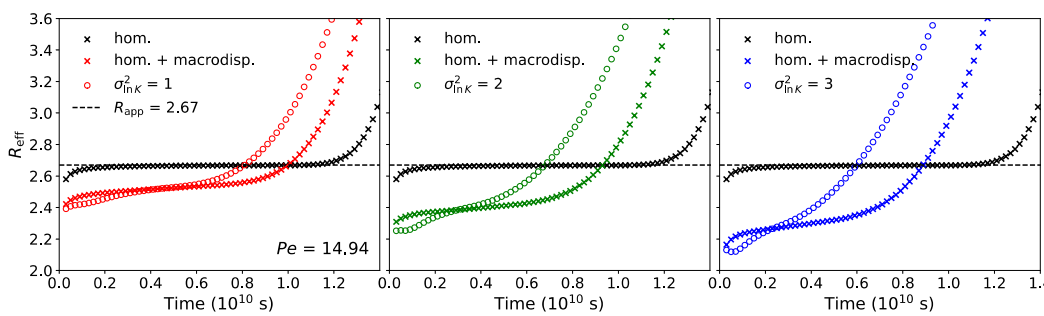

Figure 8. Temporal evolution of effective thermal retardation for the three heterogeneous cases (colored circles) compared to the homogeneous case with (colored crosses) and without (black crosses) thermal macrodispersion (scenario *L1q2*, Table 2). The dashed line indicates the value of the apparent thermal retardation factor R_{app}.

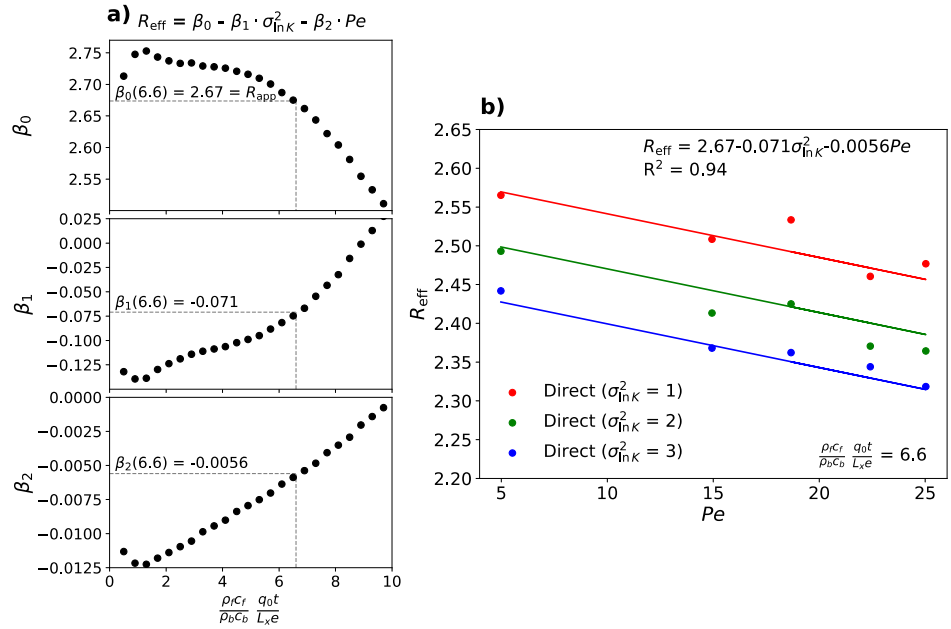

Figure 9. Results of multi-variable linear regression to derive an approximate formula for the effective thermal retardation factor R_{eff} as a function of log-conductivity variance $\sigma^2_{\ln K}$ and thermal Péclet number Pe: (a) identification of coefficients for normalized travel time $\frac{\rho_f c_f q_0 t}{\rho_b c_b L_x e} = 6.6$; (b) regression results for each log-conductivity variance, solid lines show regression curves.

in a homogeneous case by merely adjusting the effective thermal dispersion coefficient. Macrodispersion can only partially explain the change in R_{eff} caused by heterogeneity, again with differences increasing with increasing heterogeneity (Figure 8). Nonetheless, the reduction in R_{eff} relative to R_{app} can be approximately captured, at least during the initial transport phase, by incorporating macrodispersion into the homogeneous case.

3.6. A New Formula for Effective Thermal Retardation

We derive a formula that accounts for the deviation of effective retardation R_{eff} from apparent retardation R_{app} due to heterogeneity and the thermal transport regime based on the results of the temporal evolution of R_{eff} presented in Figure 7 and Figure S6 in Supporting Information S1. These results show that R_{eff} decreases at early times with increasing Péclet number in heterogeneous flow fields, which is attributed to more pronounced preferential flow and delayed local diffusion into zones of lower hydraulic conductivity. Following Chang and Yeh (2012), we rewrite the temporal evolution of R_{eff} as a function of a normalized travel time $\frac{\rho_f c_f q_0 t}{\rho_b c_b L_x e}$ for all scenarios. Details can be found in Supporting Information S1.

We perform a multi-variable linear regression using ordinary least squares for each normalized time step, where R_{eff} is treated as the response variable, and the log-conductivity variance and thermal Péclet number serve as the predictor variables (Figure 9a). All three coefficients are determined for the normalized travel time of $\frac{\rho_f c_f q_0 t}{\rho_b c_b L_x e} = 6.6$ since the absolute term β_0 of the regression curve equals the apparent thermal retardation factor of $R_{\text{app}} = 2.67$ (Figure 9a). The regression curves show a good fit with a coefficient of determination of $R^2 = 0.94$ and a root mean square error of 0.018 (Figure 9b).

Consequently, the effective thermal retardation can be estimated for heterogeneous aquifers (i.e., $\sigma^2_{\ln K} > 0$) by

$$R_{\text{eff}} = R_{\text{app}} - 0.071\,\sigma^2_{\ln K} - 0.006\,Pe, \tag{16}$$

as reduction of the apparent thermal retardation R_{app} caused by the degree of hydraulic conductivity heterogeneity $\sigma^2_{\ln K}$ and the thermal Péclet number Pe, reflecting flow velocity and characteristic length scales. Note that

Equation 16 is limited to advection-dominated regimes with $Pe > 5$, and does not incorporate the effect of porosity and pore-scale LTNE.

4. Discussion

4.1. Link to Pore-Scale LTNE

Research indicates that LTNE effects emerge at the pore scale, where significant temperature differences arise between the solid and fluid phases (Gossler et al., 2019; Hamidi et al., 2019; Heinze & Hamidi, 2017). This mostly occurs in coarse-grained materials having higher pore water velocities causing preferential flow which delays local heat diffusion into solid grains. Gossler et al. (2019) identified such effects by comparing the effective thermal retardation factor R_{eff}, being potentially influenced by pore-scale LTNE effects, with the apparent thermal retardation factor R_{app} representative for LTE. Our findings reveal that R_{eff} notably deviates from R_{app} even without considering pore-scale LTNE effects (i.e., temperature differences between the solid and fluid phases), primarily due to heterogeneous hydraulic conductivity increasing thermal velocity during the initial transport phase.

Laboratory experiments and numerical studies indicate that pore-scale LTNE effects in media with a homogeneous grain size distribution generally have a minimal impact on thermal velocities (Baek et al., 2022; Gossler et al., 2019, 2020; Shi, Wang, et al., 2024). These effects become more relevant at low Péclet numbers combined with large particle sizes, where reduced interfacial area slows heat exchange between phases. In such cases, using a pore-scale LTE model instead of a pore-scale LTNE model, which employs separate energy balance equations for the solid and fluid temperatures, results in an overestimation of thermal and flow velocities (Gossler et al., 2020; Roshan et al., 2014; Shi, Wang, et al., 2024). However, Gossler et al. (2020) and Shi, Wang, et al. (2024) showed that discrepancies in predicted thermal velocities between pore-scale LTE and LTNE models at low Péclet numbers occurred specifically under diffusion-dominated conditions and at small flow distances. In contrast, our study focuses on advection-dominated conditions with high Péclet numbers, where previous studies have consistently shown that pore-scale LTNE effects on thermal velocity are negligible (Baek et al., 2022; Gossler et al., 2019, 2020; Shi, Wang, et al., 2024). Additionally, we assume that the spatial scale considered here corresponds to time scales where the temperatures of the solid and fluid phases are in equilibrium at the pore scale. Therefore, the assumption of pore-scale LTE is justified, and pore-scale LTNE effects are unlikely to influence thermal velocities in the regimes we investigate.

In contrast, pore-scale LTNE effects can substantially impact thermal hydrodynamic dispersion (Baek et al., 2022; Gossler et al., 2019, 2020; Shi, Wang, et al., 2024). For instance, Gossler et al. (2020) found that pore-scale LTNE effects increased thermal dispersion by a factor of more than 30, while Shi, Wang, et al. (2024) reported an increase by a factor of more than 200. Since our model does not account for such effects by assuming pore-scale LTE, this represents a limitation of our study. However, such pore-scale dispersion enhancements have been observed primarily under conditions involving large grain sizes (> 7 mm according to Gossler et al. (2020)) and high flow velocities. This range of grain sizes does not apply to the sand aquifer system modeled here. Furthermore, our focus is on macrodispersivity, which is at least two orders of magnitude higher than pore-scale dispersivities (Zech et al., 2015). Given the moderate grain size and field-relevant scales of our study, the pore-scale LTE assumption remains appropriate.

Key sensitive parameters for pore-scale LTNE are Darcy velocity, particle size as characteristic length, and porosity (Gossler et al., 2020; Shi, Wang, et al., 2024). This links well to sensitive parameters we identified for LTNE at field scale, the Darcy velocity and the correlation length, as characteristic length. Both are part of the thermal Péclet number, and increases in these parameters cause a decrease in the effective thermal retardation factor R_{eff} at early times. The effect is more pronounced for changes in Darcy velocity than in correlation length.

Bandai et al. (2017) found that larger particle sizes reduce the solid-fluid surface area, leading to reduced heat exchange between the solid and fluid phases and consequently delaying heat diffusion into these particles. This observation can be linked to our findings at field scale, where the dimensions of low hydraulic conductivity zones are determined by the correlation length. Increasing the correlation lengths (L_x and L_y) enlarges the extent of low K zones, resulting in a more pronounced delay in heat diffusion into these zones. Thus, we consider heterogeneous hydraulic conductivity at the field scale as analogous to grain size distributions at pore scale in terms of LTNE effects.

4.2. Parallels to Solute Transport

Given the mathematical equivalence between the governing equations of solute and heat transport, similar effects of heterogeneity on transport and spreading can be anticipated. For reactive solute transport with linear chemical adsorption, increasing heterogeneity is expected to reduce effective solute retardation factors. However, Dagan and Cvetkovic (1993) showed theoretically that, for a kinetically sorbing solute injected instantaneously, the mass and mean centroid coordinate of the solute plume are unaffected by the variance of the heterogeneous hydraulic conductivity but depend on the mean flow velocity. In contrast, our results show that increasing log-conductivity variance substantially affects effective thermal retardation factors being the analog of the solute retardation factor. Getting more insights into the analogy between heat and reactive solute transport would require extending our modeling framework to reactive solute transport with different boundary conditions (instantaneous point injection instead of continuous line source injection), which is beyond the scope of this study.

4.3. Implications for Heat Tracer Testing and Geothermal Systems

The deviation between effective and apparent thermal retardation factors due to field-scale LTNE effects holds implications for subsurface heat applications. For example, heat tracer experiments are often conducted to estimate water fluxes in streambeds (e.g., Anderson, 2005; Constantz, 2008; Halloran et al., 2016; Kurylyk et al., 2019; Rau et al., 2014). While pore-scale LTNE effects are unlikely to substantially impact water flux estimates (Gossler et al., 2020), our results indicate that incorporating field-scale LTNE effects can improve the accuracy of these estimates.

Previous studies about the effect of streambed heterogeneity on temperature-based water flux calculations showed that errors in flux estimates tend to increase with the degree of heterogeneity (Irvine, Cranswick, et al., 2015; Schornberg et al., 2010) by comparing one-dimensional analytical solutions with numerical simulations. Their analytical solutions include a thermal velocity that is based on an apparent thermal retardation factor R_{app}. Adjusting the thermal retardation factor to account for log-conductivity variance and thermal Pe using Equation 16 can reduce errors in these flux estimates. Using R_{app} without accounting for field-scale LTNE effects leads to an overestimation of thermal retardation and consequently causes an overestimation of water fluxes derived from temperature data. Equation 16 further shows that the effect of the log-conductivity variance on the reduction of R_{app} is approximately 12 times stronger than that of the thermal Péclet number, underscoring the dominant role of heterogeneity in controlling thermal retardation.

Coupled heat and solute tracer tests for aquifer characterization and estimation of heat transfer parameters (e.g., Colombani et al., 2015; Constantz et al., 2003; Hoffmann et al., 2019; Ma et al., 2012; Sarris et al., 2018; Vandenbohede et al., 2009; Wildemeersch et al., 2014) offer valuable insights into field-specific conditions. They have the potential to assess the suitability of Equation 16 for approximating R_{eff}. Hoffmann et al. (2019) found that assuming a thermal retardation factor based on spatially uniform (i.e., fixed) specific heat capacities was insufficient to account for heterogeneity present within the strongly advective aquifer environment of their test site. Therefore, they applied a thermal retardation factor of one, reflecting conservative transport conditions and indicating that R_{eff} can be substantially lower than R_{app} under field conditions, with R_{app} estimated to be approximately 4.6 based on the parameter values given by Hoffmann et al. (2019). Similarly, Colombani et al. (2015) set the thermal retardation factor to one during the calibration of their numerical model to align with the BTCs observed in their coupled heat and saline tracer experiment under a forced hydraulic gradient.

Our results align with research findings on the impact of heterogeneity on the efficiency of geothermal systems, in particular aquifer thermal energy storage (ATES) systems (e.g., Bridger & Allen, 2010; Ferguson, 2007; Sommer et al., 2013, 2014; Tang & van der Zee, 2022). Recovery efficiency in ATES systems is typically defined as the fraction of injected thermal energy that is recovered during the extraction phase, calculated as the ratio of the total extracted thermal energy to the total injected thermal energy, both relative to the ambient groundwater temperature (Bloemendal & Hartog, 2018; Sommer et al., 2013, 2014). As we showed, thermal retardation reduces with increasing heterogeneity during the initial transport phase, primarily due to preferential flow. Preferential flow pathways lead to a larger area-to-volume ratio of the injected thermal plume, which influences recovery efficiency of ATES systems (Tang & van der Zee, 2022). Short-circuiting and thermal interference due to preferential flow pathways further reduce ATES performance (Bridger & Allen, 2010; Sommer et al., 2013, 2014).

Equation 16 provides an option to improve recovery efficiency prediction in ATES systems by using a better estimate for the thermal retardation factor R_{eff}. Bloemendal and Hartog (2018) demonstrated that high ambient groundwater flow affects the recovery efficiency of ATES systems substantially. Heat losses due to displacement depend on thermal velocity, typically approximated as the ratio of seepage velocity and apparent thermal retardation (v_a/R_{app}). Using an effective thermal retardation factor taking heterogeneity into account further increases thermal velocities and displacement of heat, particularly during the initial phase of injection. This has practical implications, as mitigating displacement losses require minimizing the well screen length or maximizing the stored volume (Bloemendal & Hartog, 2018).

4.4. Limitations of the Present Approach and Future Directions

The modeling approach used in this study incorporates spatially heterogeneous hydraulic conductivity while keeping the remaining properties constant and assumes pore-scale LTE. This approach is supported by the literature and suitable for advection-dominated regimes in sedimentary aquifers but inevitably involves simplifications that impose certain limitations.

First, the framework does not consider spatial variability of porosity, thereby omitting potential feedbacks from heterogeneity of this property. In particular, several studies investigating contaminant transport have shown that porosity heterogeneity, when positively correlated with K, can influence solute transport behavior and uncertainty, affecting BTC arrival times and plume spreading (Hassan et al., 1998; Hu et al., 2009; Libera et al., 2019; Riva et al., 2008). Although porosity in unconsolidated sediments generally varies less than K, a co-variation of K and porosity may influence transport dynamics in certain heat transport scenarios.

Similarly, while heterogeneity in thermal conductivity is considered secondary in aquifers with smoothly varying sediment properties, it may become more important in settings with sharp lithological contrasts, especially under conduction-dominated systems (Fulton & Saffer, 2009). This influence has been explored in prior studies of heterogeneous sedimentary aquifers: Markle et al. (2006) observed increased thermal dispersion near plume fronts in simulations with heterogeneous thermal conductivity, whereas Sebok and Müller (2019) and Seibert et al. (2014) found that assuming spatially uniform thermal properties was generally sufficient to accurately simulate temperature dynamics.

Second, our model assumes pore-scale LTE, which may underestimate thermal spreading, as previous studies have demonstrated that incorporating pore-scale LTNE effects can significantly enhance thermal dispersion (Gossler et al., 2020; Shi, Wang, et al., 2024), as discussed in Section 4.1.

Future work may focus on co-varying fields of K and porosity, for example, by incorporating positive correlations between these parameters. Likewise, adopting binary or zonated field representations that jointly vary K, porosity, bulk thermal conductivity, and heat capacity would better capture lithological contrasts, as opposed to the relatively smooth K transitions considered here. This can be further integrated into multi-scale modeling frameworks that solve the two-phase energy equations for fluid and solid phases to capture potential pore-scale LTNE effects. Exploring a broader range of Péclet numbers, especially for $Pe < 1$, would better characterize thermal LTNE effects at both pore and field scales across varying thermal regimes. Additionally, there is strong potential for improving understanding of field-scale LTNE not only through simulations but also through combined heat and solute tracer experiments. In particular, systematically comparing thermal and solute transport velocities from field tracer data could yield valuable insights into actual subsurface transport processes and help validate estimates of R_{eff} under site-specific conditions. However, these extensions are beyond the scope of this study, which focuses on isolating and quantifying the influence of K heterogeneity on field-scale LTNE effects.

5. Summary and Conclusions

This study investigated the relationship between macro-scale heterogeneity, thermal retardation, and dispersion during heat transport in aquifers. We developed a stochastic model of heterogeneous hydraulic conductivity K to numerically simulate the transient evolution of a heat plume generated by a line-like heat source within a three-dimensional aquifer. To characterize the transient heat plume evolution, we examined scale-dependent longitudinal thermal dispersion coefficients $D_L(x)$ and time-dependent effective thermal retardation factors R_{eff}. We identified the effect of heterogeneity on R_{eff} through varying the log-hydraulic conductivity variance $\sigma^2_{\ln K}$ and

explored the influence of the thermal Péclet number Pe on R_{eff} by adjusting both the Darcy velocity and the correlation length of the log-conductivity field.

A key finding is that with increasing hydraulic conductivity heterogeneity and thermal Pe, effective thermal retardation R_{eff} becomes lower than apparent thermal retardation R_{app}, by up to 14% in the most heterogeneous ($\sigma^2_{\ln K} = 3$) and most advective cases ($Pe = 25.03$) considered. The main cause is higher thermal velocities at early times, caused by preferential flow in high-K zones and delayed heat diffusion in low-K zones. We termed the deviation of R_{eff} from R_{app} in spatially heterogeneous aquifers as "field-scale local thermal non-equilibrium (LTNE)" and derived a formula to estimate R_{eff} as a function of aquifer heterogeneity parameters and flow velocity.

From our findings we draw the main conclusions:

- The effect of heterogeneity (expressed through log-hydraulic conductivity variance $\sigma^2_{\ln K}$) is about 12 times stronger than that of flow velocity (expressed through the thermal Péclet number Pe) in reducing apparent thermal retardation R_{app}.
- The effect of field-scale LTNE cannot be captured solely by adding thermal macrodispersion in simulations with homogeneous flow fields. While this approach replicates the heterogeneity-induced decrease in thermal retardation at early times, discrepancies with heterogeneous cases increase over time and with greater heterogeneity. It also leads to enhanced longitudinal plume spreading during later times before steady-state is reached.
- Key sensitive parameters for field scale LTNE effects align well with those found for pore-scale LTNE: flow velocity and a characteristic length scale—being particle size at pore scale and correlation length at field scale.
- Using an adjusted thermal retardation factor accounting for aquifer heterogeneity will enhance the accuracy of flux estimates using heat tracer techniques and predictions of recovery efficiency in ATES systems.

We see high potential for more research on field-scale LTNE effects. Direct next steps will include (a) a systematic comparison between thermal and solute transport velocities through joint heat and solute tracer field experiments to identify field-specific conditions and validate the formula for estimating R_{eff}; (b) investigating the field-scale LTNE effect across a broader range of thermal Péclet numbers, particularly for $Pe < 1$, to gain understanding of diffusion-dominated thermal regimes. Moreover, using multi-scale numerical models are an option to effectively integrate pore-scale LTNE and study their effects on hydrodynamic dispersion with field-scale LTNE effects and macrodispersion.

Acronyms

ATES	Aquifer thermal energy storage
BHE	Borehole heat exchanger
BTC	Breakthrough curve
LTE	Local thermal equilibrium
LTNE	Local thermal non-equilibrium
RMSE	Root mean square error

Conflict of Interest

The authors declare no conflicts of interest relevant to this study.

Data Availability Statement

The result data set and the Python and MOOSE scripts used to create the data set of this study are available at Zenodo (doi: https://doi.org/10.5281/zenodo.14793523) (Gebhardt, 2025).

Acknowledgments
This work was supported by the German Research Foundation (DFG) based on grant number BA 2850/8-1 (project number 468464290). The authors thank the editors, Quanrong Wang, and the anonymous reviewer for their thorough assessment and constructive comments. The authors also thank Ryan Pearson for proofreading. Open Access funding enabled and organized by Projekt DEAL.

References

Amiri, V., Sohrabi, N., Li, P., & Shukla, S. (2023). Estimation of hydraulic conductivity and porosity of a heterogeneous porous aquifer by combining transition probability geostatistical simulation, geophysical survey, and pumping test data. *Environment, Development and Sustainability*, *25*(8), 7713–7736. https://doi.org/10.1007/s10668-022-02368-6

Anderson, M. P. (2005). Heat as a ground water tracer. *Groundwater*, *43*(6), 951–968. https://doi.org/10.1111/j.1745-6584.2005.00052.x

Attinger, S., Dentz, M., Kinzelbach, H., & Kinzelbach, W. (1999). Temporal behaviour of a solute cloud in a chemically heterogeneous porous medium. *Journal of Fluid Mechanics*, *386*, 77–104. https://doi.org/10.1017/S0022112099004334

Baek, J.-Y., Park, B.-H., Rau, G. C., & Lee, K.-K. (2022). Experimental evidence for local thermal non-equilibrium during heat transport in sand representative of natural conditions. *Journal of Hydrology*, *608*, 127589. https://doi.org/10.1016/j.jhydrol.2022.127589

Baek, J.-Y., Park, B.-H., Rau, G. C., & Lee, K.-K. (2024). Experiments reveal effects of particle and pore-scale heterogeneity on thermal dispersion during porous media heat transport. *Journal of Hydrology*, *639*, 131568. https://doi.org/10.1016/j.jhydrol.2024.131568

Bandai, T., Hamamoto, S., Rau, G. C., Komatsu, T., & Nishimura, T. (2017). The effect of particle size on thermal and solute dispersion in saturated porous media. *International Journal of Thermal Sciences*, *122*, 74–84. https://doi.org/10.1016/j.ijthermalsci.2017.08.003

Bastías Espejo, J. M., Wilkins, A., Rau, G. C., & Blum, P. (2021). Rhea v1.0: Enabling fully coupled simulations with hydro-geomechanical heterogeneity. *Geoscientific Model Development*, *14*(10), 6257–6272. https://doi.org/10.5194/gmd-14-6257-2021

Bertagnoli, A., Luce, C., van Kampen, R., Schneidewind, U., van Berkel, M., Tranmer, A. W., et al. (2024). iflow: A framework and gui to quantify effective thermal diffusivity and advection in permeable materials from temperature time series. *Water Resources Research*, *60*(11), e2024WR037370. https://doi.org/10.1029/2024WR037370

Bloemendal, M., & Hartog, N. (2018). Analysis of the impact of storage conditions on the thermal recovery efficiency of low-temperature ates systems. *Geothermics*, *71*, 306–319. https://doi.org/10.1016/j.geothermics.2017.10.009

Bridger, D. W., & Allen, D. M. (2010). Heat transport simulations in a heterogeneous aquifer used for aquifer thermal energy storage (ates). *Canadian Geotechnical Journal*, *47*(1), 96–115. https://doi.org/10.1139/T09-078

Burr, D. T., Sudicky, E. A., & Naff, R. L. (1994). Nonreactive and reactive solute transport in three–dimensional heterogeneous porous media: Mean displacement, plume spreading, and uncertainty. *Water Resources Research*, *30*(3), 791–815. https://doi.org/10.1029/93WR02946

Chang, C.-M., & Yeh, H.-D. (2012). Stochastic analysis of field-scale heat advection in heterogeneous aquifers. *Hydrology and Earth System Sciences*, *16*(3), 641–648. https://doi.org/10.5194/hess-16-641-2012

Colombani, N., Giambastiani, B., & Mastrocicco, M. (2015). Combined use of heat and saline tracer to estimate aquifer properties in a forced gradient test. *Journal of Hydrology*, *525*, 650–657. https://doi.org/10.1016/j.jhydrol.2015.04.026

Constantz, J. (2008). Heat as a tracer to determine streambed water exchanges. *Water Resources Research*, *44*(4), W00D10. https://doi.org/10.1029/2008WR006996

Constantz, J., Cox, M. H., & Su, G. W. (2003). Comparison of heat and bromide as ground water tracers near streams. *Groundwater*, *41*(5), 647–656. https://doi.org/10.1111/j.1745-6584.2003.tb02403.x

Dagan, G. (1986). Statistical theory of groundwater flow and transport: Pore to laboratory, laboratory to formation, and formation to regional scale. *Water Resources Research*, *22*(9S), 120S–134S. https://doi.org/10.1029/WR022i09Sp0120S

Dagan, G. (1989). *Flow and transport in porous formations*. Springer Berlin Heidelberg.

Dagan, G. (1990). Transport in heterogeneous porous formations: Spatial moments, ergodicity, and effective dispersion. *Water Resources Research*, *26*(6), 1281–1290. https://doi.org/10.1029/WR026i006p01281

Dagan, G., & Cvetkovic, V. (1993). Spatial moments of a kinetically sorbing solute plume in a heterogeneous aquifer. *Water Resources Research*, *29*(12), 4053–4061. https://doi.org/10.1029/93WR02299

de Marsily, G. (1986). *Quantitative hydrogeology: Groundwater hydrology for engineers*. Paris School of Mines.

Dentz, M., Kinzelbach, H., Attinger, S., & Kinzelbach, W. (2000). Temporal behavior of a solute cloud in a heterogeneous porous medium: 1. Point–like injection. *Water Resources Research*, *36*(12), 3591–3604. https://doi.org/10.1029/2000WR900162

Doro, K. O., Cirpka, O. A., & Leven, C. (2015). Tracer tomography: Design concepts and field experiments using heat as a tracer. *Groundwater*, *53*(S1), 139–148. https://doi.org/10.1111/gwat.12299

Ferguson, G. (2007). Heterogeneity and thermal modeling of ground water. *Groundwater*, *45*(4), 485–490. https://doi.org/10.1111/j.1745-6584.2007.00323.x

Freeze, R. A., & Cherry, J. A. (1979). *Groundwater*. Prentice-Hall.

Fulton, P. M., & Saffer, D. M. (2009). Effect of thermal refraction on heat flow near the San Andreas Fault, Parkfield, California. *Journal of Geophysical Research*, *114*, B06408. https://doi.org/10.1029/2008JB005796

Furlanetto, D., Camporese, M., Schenato, L., Costa, L., & Salandin, P. (2024). Fiber optics passive monitoring of groundwater temperature reveals three-dimensional structures in heterogeneous aquifers. *Scientific Reports*, *14*(1), 8430. https://doi.org/10.1038/s41598-024-58954-3

Gaston, D., Newman, C., Hansen, G., & Lebrun-Grandié, D. (2009). Moose: A parallel computational framework for coupled systems of nonlinear equations. *Nuclear Engineering and Design*, *239*(10), 1768–1778. https://doi.org/10.1016/j.nucengdes.2009.05.021

Gebhardt, H. (2025). hannahgeb/thermalretardation_ltne: February 3, 2025 Release (Version 1.0.0) [Software]. *Zenodo*. https://doi.org/10.5281/zenodo.14793523

Gelhar, L. W. (1986). Stochastic subsurface hydrology from theory to applications. *Water Resources Research*, *22*(9S), 135S–145S. https://doi.org/10.1029/WR022i09Sp0135S

Gelhar, L. W., & Axness, C. L. (1983). Three–dimensional stochastic analysis of macrodispersion in aquifers. *Water Resources Research*, *19*(1), 161–180. https://doi.org/10.1029/WR019i001p00161

Gelhar, L. W., Welty, C., & Rehfeldt, K. R. (1992). A critical review of data on field–scale dispersion in aquifers. *Water Resources Research*, *28*(7), 1955–1974. https://doi.org/10.1029/92WR00607

Gossler, M. A., Bayer, P., Rau, G. C., Einsiedl, F., & Zosseder, K. (2020). On the limitations and implications of modeling heat transport in porous aquifers by assuming local thermal equilibrium. *Water Resources Research*, *56*(10), e2020WR027772. https://doi.org/10.1029/2020WR027772

Gossler, M. A., Bayer, P., & Zosseder, K. (2019). Experimental investigation of thermal retardation and local thermal non-equilibrium effects on heat transport in highly permeable, porous aquifers. *Journal of Hydrology*, *578*, 124097. https://doi.org/10.1016/j.jhydrol.2019.124097

Green, D. W., Perry, R. H., & Babcock, R. E. (1964). Longitudinal dispersion of thermal energy through porous media with a flowing fluid. *AIChE Journal*, *10*(5), 645–651. https://doi.org/10.1002/aic.690100514

Hähnlein, S., Bayer, P., Ferguson, G., & Blum, P. (2013). Sustainability and policy for the thermal use of shallow geothermal energy. *Energy Policy*, *59*, 914–925. https://doi.org/10.1016/j.enpol.2013.04.040

Halloran, L. J., Rau, G. C., & Andersen, M. S. (2016). Heat as a tracer to quantify processes and properties in the Vadose zone: A review. *Earth-Science Reviews*, *159*, 358–373. https://doi.org/10.1016/j.earscirev.2016.06.009

Hamidi, S., Heinze, T., Galvan, B., & Miller, S. (2019). Critical review of the local thermal equilibrium assumption in heterogeneous porous media: Dependence on permeability and porosity contrasts. *Applied Thermal Engineering*, *147*, 962–971. https://doi.org/10.1016/j.applthermaleng.2018.10.130

Hassan, A. E., Cushman, J. H., & Delleur, J. W. (1998). Significance of porosity variability to transport in heterogeneous porous media. *Water Resources Research*, *34*(9), 2249–2259. https://doi.org/10.1029/98WR01470

Haynes, W. M., Lide, D. R., & Bruno, T. J. (Eds.). (2016). *CRC handbook of chemistry and physics*. CRC Press. https://doi.org/10.1201/9781315380476

Hecht-Méndez, J., Molina-Giraldo, N., Blum, P., & Bayer, P. (2010). Evaluating mt3dms for heat transport simulation of closed geothermal systems. *Groundwater*, *48*(5), 741–756. https://doi.org/10.1111/j.1745-6584.2010.00678.x

Heinze, T. (2024). Multi-phase heat transfer in porous and fractured rock. *Earth-Science Reviews*, *251*, 104730. https://doi.org/10.1016/j.earscirev.2024.104730

Heinze, T., & Blöcher, J. R. (2019). A model of local thermal non-equilibrium during infiltration. *Advances in Water Resources*, *132*, 103394. https://doi.org/10.1016/j.advwatres.2019.103394

Heinze, T., & Hamidi, S. (2017). Heat transfer and parameterization in local thermal non-equilibrium for dual porosity continua. *Applied Thermal Engineering*, *114*, 645–652. https://doi.org/10.1016/j.applthermaleng.2016.12.015

Hidalgo, J. J., Carrera, J., & Dentz, M. (2009). Steady state heat transport in 3d heterogeneous porous media. *Advances in Water Resources*, *32*(8), 1206–1212. https://doi.org/10.1016/j.advwatres.2009.04.003

Hoffmann, R., Dassargues, A., Goderniaux, P., & Hermans, T. (2019). Heterogeneity and prior uncertainty investigation using a joint heat and solute tracer experiment in alluvial sediments. *Frontiers in Earth Science*, *7*. https://doi.org/10.3389/feart.2019.00108

Hu, B. X., Meerschaert, M. M., Barrash, W., Hyndman, D. W., He, C., Li, X., & Guo, L. (2009). Examining the influence of heterogeneous porosity fields on conservative solute transport. *Journal of Contaminant Hydrology*, *108*(3–4), 77–88. https://doi.org/10.1016/j.jconhyd.2009.06.001

Irvine, D. J., Cranswick, R. H., Simmons, C. T., Shanafield, M. A., & Lautz, L. K. (2015). The effect of streambed heterogeneity on groundwater-surface water exchange fluxes inferred from temperature time series. *Water Resources Research*, *51*(1), 198–212. https://doi.org/10.1002/2014WR015769

Irvine, D. J., Simmons, C. T., Werner, A. D., & Graf, T. (2015). Heat and solute tracers: How do they compare in heterogeneous aquifers? *Groundwater*, *53*(S1), 10–20. https://doi.org/10.1111/gwat.12146

KarisAllen, J. J., Mohammed, A. A., Tamborski, J. J., Jamieson, R. C., Danielescu, S., & Kurylyk, B. L. (2022). Present and future thermal regimes of intertidal groundwater springs in a threatened coastal ecosystem. *Hydrology and Earth System Sciences*, *26*(18), 4721–4740. https://doi.org/10.5194/hess-26-4721-2022

Kaviany, M. (1995). *Principles of heat transfer in porous media*. Springer New York. https://doi.org/10.1007/978-1-4612-4254-3

Kitanidis, P. K. (1988). Prediction by the method of moments of transport in a heterogeneous formation. *Journal of Hydrology*, *102*(1–4), 453–473. https://doi.org/10.1016/0022-1694(88)90111-4

Klepikova, M., Wildemeersch, S., Hermans, T., Jamin, P., Orban, P., Nguyen, F., et al. (2016). Heat tracer test in an alluvial aquifer: Field experiment and inverse modelling. *Journal of Hydrology*, *540*, 812–823. https://doi.org/10.1016/j.jhydrol.2016.06.066

Kurylyk, B. L., Irvine, D. J., & Bense, V. F. (2019). Theory, tools, and multidisciplinary applications for tracing groundwater fluxes from temperature profiles. *WIREs Water*, *6*(1), e1329. https://doi.org/10.1002/wat2.1329

Kurylyk, B. L., MacQuarrie, K. T., & McKenzie, J. M. (2014). Climate change impacts on groundwater and soil temperatures in cold and temperate regions: Implications, mathematical theory, and emerging simulation tools. *Earth-Science Reviews*, *138*, 313–334. https://doi.org/10.1016/j.earscirev.2014.06.006

Kurylyk, B. L., MacQuarrie, K. T. B., Linnansaari, T., Cunjak, R. A., & Curry, R. A. (2015). Preserving, augmenting, and creating cold–water thermal refugia in rivers: Concepts derived from research on the Miramichi River, New Brunswick (Canada). *Ecohydrology*, *8*(6), 1095–1108. https://doi.org/10.1002/eco.1566

Levec, J., & Carbonell, R. G. (1985). Longitudinal and lateral thermal dispersion in packed beds. part ii: Comparison between theory and experiment. *AIChE Journal*, *31*(4), 591–602. https://doi.org/10.1002/aic.690310409

Libera, A., Henri, C. V., & De Barros, F. P. (2019). Hydraulic conductivity and porosity heterogeneity controls on environmental performance metrics: Implications in probabilistic risk analysis. *Advances in Water Resources*, *127*, 1–12. https://doi.org/10.1016/j.advwatres.2019.03.002

Ma, R., Zheng, C., Zachara, J. M., & Tonkin, M. (2012). Utility of bromide and heat tracers for aquifer characterization affected by highly transient flow conditions. *Water Resources Research*, *48*(8), W08523. https://doi.org/10.1029/2011WR011281

Markle, J. M., Schincariol, R. A., Sass, J. H., & Molson, J. W. (2006). Characterizing the two–dimensional thermal conductivity distribution in a sand and gravel aquifer. *Soil Science Society of America Journal*, *70*(4), 1281–1294. https://doi.org/10.2136/sssaj2005.0293

Molnár, B., Lenkey, L., Pedretti, D., Mádl-Szőnyi, J., & Galsa, A. (2025). Elucidating the relationship between aquifer heterogeneity and thermal dispersivity using stochastic heat transport simulations. *Hydrogeology Journal*, *33*(2), 493–513. https://doi.org/10.1007/s10040-025-02875-6

Müller, S., Schüler, L., Zech, A., & Heße, F. (2022). Gstools v1.3: A toolbox for geostatistical modelling in python. *Geoscientific Model Development*, *15*(7), 3161–3182. https://doi.org/10.5194/gmd-15-3161-2022

Park, B.-H., Bae, G.-O., & Lee, K.-K. (2015). Importance of thermal dispersivity in designing groundwater heat pump (gwhp) system: Field and numerical study. *Renewable Energy*, *83*, 270–279. https://doi.org/10.1016/j.renene.2015.04.036

Park, B.-H., Lee, B.-H., & Lee, K.-K. (2018). Experimental investigation of the thermal dispersion coefficient under forced groundwater flow for designing an optimal groundwater heat pump (gwhp) system. *Journal of Hydrology*, *562*, 385–396. https://doi.org/10.1016/j.jhydrol.2018.05.023

Pastore, N., Cherubini, C., Rapti, D., & Giasi, C. I. (2018). Experimental study of forced convection heat transport in porous media. *Nonlinear Processes in Geophysics*, *25*(2), 279–290. https://doi.org/10.5194/npg-25-279-2018

Permann, C. J., Gaston, D. R., Andrš, D., Carlsen, R. W., Kong, F., Lindsay, A. D., et al. (2020). Moose: Enabling massively parallel multiphysics simulation. *SoftwareX*, *11*, 100430. https://doi.org/10.1016/j.softx.2020.100430

Pophillat, W., Bayer, P., Teyssier, E., Blum, P., & Attard, G. (2020). Impact of groundwater heat pump systems on subsurface temperature under variable advection, conduction and dispersion. *Geothermics*, *83*, 101721. https://doi.org/10.1016/j.geothermics.2019.101721

Rajaram, H. (1997). Time and scale dependent effective retardation factors in heterogeneous aquifers. *Advances in Water Resources*, *20*(4), 217–230. https://doi.org/10.1016/S0309-1708(96)00021-8

Rau, G. C., Andersen, M. S., & Acworth, R. I. (2012). Experimental investigation of the thermal dispersivity term and its significance in the heat transport equation for flow in sediments. *Water Resources Research*, *48*(3), W03511. https://doi.org/10.1029/2011WR011038

Rau, G. C., Andersen, M. S., McCallum, A. M., Roshan, H., & Acworth, R. I. (2014). Heat as a tracer to quantify water flow in near-surface sediments. *Earth-Science Reviews*, *129*, 40–58. https://doi.org/10.1016/j.earscirev.2013.10.015

Riva, M., Guadagnini, A., Fernandez-Garcia, D., Sanchez-Vila, X., & Ptak, T. (2008). Relative importance of geostatistical and transport models in describing heavily tailed breakthrough curves at the lauswiesen site. *Journal of Contaminant Hydrology*, *101*(1–4), 1–13. https://doi.org/10.1016/j.jconhyd.2008.07.004

Roshan, H., Cuthbert, M. O., Andersen, M. S., & Acworth, R. I. (2014). Local thermal non-equilibrium in sediments: Implications for temperature dynamics and the use of heat as a tracer. *Advances in Water Resources*, *73*, 176–184. https://doi.org/10.1016/j.advwatres.2014.08.002

Sarris, T. S., Close, M., & Abraham, P. (2018). Using solute and heat tracers for aquifer characterization in a strongly heterogeneous alluvial aquifer. *Journal of Hydrology*, *558*, 55–71. https://doi.org/10.1016/j.jhydrol.2018.01.032

Sauty, J. P., Gringarten, A. C., Fabris, H., Thiery, D., Menjoz, A., & Landel, P. A. (1982). Sensible energy storage in aquifers: 2. Field experiments and comparison with theoretical results. *Water Resources Research*, *18*(2), 253–265. https://doi.org/10.1029/WR018i002p00253

Schön, J. H. (1996). *Physical properties of rocks: Fundamentals and principles of petrophysics*. Pergamon.

Schornberg, C., Schmidt, C., Kalbus, E., & Fleckenstein, J. H. (2010). Simulating the effects of geologic heterogeneity and transient boundary conditions on streambed temperatures—Implications for temperature-based water flux calculations. *Advances in Water Resources*, *33*(11), 1309–1319. https://doi.org/10.1016/j.advwatres.2010.04.007

Sebok, E., & Müller, S. (2019). The effect of sediment thermal conductivity on vertical groundwater flux estimates. *Hydrology and Earth System Sciences*, *23*(8), 3305–3317. https://doi.org/10.5194/hess-23-3305-2019

Seibert, S., Prommer, H., Siade, A., Harris, B., Trefry, M., & Martin, M. (2014). Heat and mass transport during a groundwater replenishment trial in a highly heterogeneous aquifer. *Water Resources Research*, *50*(12), 9463–9483. https://doi.org/10.1002/2013WR015219

Shi, W., Wang, Q., Klepikova, M., & Zhan, H. (2024). New criteria to estimate local thermal nonequilibrium conditions for heat transport in porous aquifers. *Water Resources Research*, *60*(7), e2024WR037382. https://doi.org/10.1029/2024WR037382

Shi, W., Zhan, H., Wang, Q., & Liao, Z. (2024). Quantifying vertical streambed fluxes and streambed thermal properties using heat as a tracer during extreme hydrologic events. *Journal of Hydrology*, *629*, 130553. https://doi.org/10.1016/j.jhydrol.2023.130553

Sommer, W., Valstar, J., van Gaans, P., Grotenhuis, T., & Rijnaarts, H. (2013). The impact of aquifer heterogeneity on the performance of aquifer thermal energy storage. *Water Resources Research*, *49*(12), 8128–8138. https://doi.org/10.1002/2013WR013677

Sommer, W. T., Doornenbal, P. J., Drijver, B. C., van Gaans, P. F. M., Leusbrock, I., Grotenhuis, J. T. C., & Rijnaarts, H. H. M. (2014). Thermal performance and heat transport in aquifer thermal energy storage. *Hydrogeology Journal*, *22*(1), 263–279. https://doi.org/10.1007/s10040-013-1066-0

Somogyvári, M., & Bayer, P. (2017). Field validation of thermal tracer tomography for reconstruction of aquifer heterogeneity. *Water Resources Research*, *53*(6), 5070–5084. https://doi.org/10.1002/2017WR020543

Sözen, M., & Vafai, K. (1990). Analysis of the non-thermal equilibrium condensing flow of a gas through a packed bed. *International Journal of Heat and Mass Transfer*, *33*(6), 1247–1261. https://doi.org/10.1016/0017-9310(90)90255-S

Stauffer, F., Bayer, P., Blum, P., Giraldo, N. M., & Kinzelbach, W. (2014). *Thermal use of shallow groundwater*. CRC Press.

Sudicky, E. A. (1986). A natural gradient experiment on solute transport in a sand aquifer: Spatial variability of hydraulic conductivity and its role in the dispersion process. *Water Resources Research*, *22*(13), 2069–2082. https://doi.org/10.1029/WR022i013p02069

Tang, D. W. S., & van der Zee, S. E. A. T. M. (2022). Macrodispersion and recovery of solutes and heat in heterogeneous aquifers. *Water Resources Research*, *58*(2), e2021WR030920. https://doi.org/10.1029/2021WR030920

Tompson, A. F. B., & Gelhar, L. W. (1990). Numerical simulation of solute transport in three–dimensional, randomly heterogeneous porous media. *Water Resources Research*, *26*(10), 2541–2562. https://doi.org/10.1029/WR026i010p02541

Vandenbohede, A., Louwyck, A., & Lebbe, L. (2009). Conservative solute versus heat transport in porous media during push-pull tests. *Transport in Porous Media*, *76*(2), 265–287. https://doi.org/10.1007/s11242-008-9246-4

van Genuchten, M. T., & Alves, W. J. (1982). *Analytical solutions of the one-dimensional convective-dispersive solute transport equation (Technical Bulletin No. 1661)*. U.S. Department of Agriculture.

Wagner, V., Li, T., Bayer, P., Leven, C., Dietrich, P., & Blum, P. (2014). Thermal tracer testing in a sedimentary aquifer: Field experiment (Lauswiesen, Germany) and numerical simulation. *Hydrogeology Journal*, *22*(1), 175–187. https://doi.org/10.1007/s10040-013-1059-z

Whitaker, S. (1991). Improved constraints for the principle of local thermal equilibrium. *Industrial & Engineering Chemistry Research*, *30*(5), 983–997. https://doi.org/10.1021/ie00053a022

Wildemeersch, S., Jamin, P., Orban, P., Hermans, T., Klepikova, M., Nguyen, F., et al. (2014). Coupling heat and chemical tracer experiments for estimating heat transfer parameters in shallow alluvial aquifers. *Journal of Contaminant Hydrology*, *169*, 90–99. https://doi.org/10.1016/j.jconhyd.2014.08.001

Wilkins, A., Green, C. P., & Ennis-King, J. (2020). Porousflow: A multiphysics simulation code for coupled problems in porous media. *Journal of Open Source Software*, *5*(55), 2176. https://doi.org/10.21105/joss.02176

Wilkins, A., Green, C. P., & Ennis-King, J. (2021). An open-source multiphysics simulation code for coupled problems in porous media. *Computers & Geosciences*, *154*, 104820. https://doi.org/10.1016/j.cageo.2021.104820

Zech, A., Attinger, S., Cvetkovic, V., Dagan, G., Dietrich, P., Fiori, A., et al. (2015). Is unique scaling of aquifer macrodispersivity supported by field data? *Water Resource Research*, *51*(9), 7662–7679. https://doi.org/10.1002/2015WR017220

References From the Supporting Information

Ababou, R., McLaughlin, D., Gelhar, L. W., & Tompson, A. F. (1989). Numerical simulation of three-dimensional saturated flow in randomly heterogeneous porous media. *Transport in Porous Media*, *4*(6), 549–565. https://doi.org/10.1007/BF00223627

Carslaw, H. S., & Jaeger, J. C. (1959). *Conduction of heat in solids* (2nd ed.). Oxford University Press.